Article

Numerical and Experimental Study on the Process of Filling Water in Pressurized Water Pipeline

Jianyong Hu [1,2], Qingbo Wang [1,3], Yuzhou Zhang [1,2,*], Zhenzhu Meng [2,4], Jinxin Zhang [2,4] and Jiarui Fan [5]

1   School of Geomatics and Municipal Engineering, Zhejiang University of Water Resources and Electric Power, Hangzhou 310018, China; hujy@zjweu.edu.cn (J.H.); wangqb@zjweu.edu.cn (Q.W.)
2   Engineering Research Center of Digital Twin Basin of Zhejiang Province, Hangzhou 310018, China; mengzhzh@zjweu.edu.cn (Z.M.); zhangjx@zjweu.edu.cn (J.Z.)
3   School of Electric Power, North China University of Water Resources and Hydropower, Zhengzhou 450045, China
4   School of Water Conservancy and Environment Engineering, Zhejiang University of Water Resources and Electric Power, Hangzhou 310018, China
5   Northwest Electric Power Design Institute of China Power Engineering Consulting Group, Xi'an 710000, China; fanjr@zjweu.edu.cn
*   Correspondence: zhangyzh@zjweu.edu.cn

Abstract: As an important working condition in water conveyance projects, the water filling process of pipelines is a complex hydraulic transition process involving water–air two-phase flow with sharp pressure changes that can easily cause pipeline damage. In light of the complex water–air two-phase flow during pipeline water filling, this study explores the water filling process of right-angle elbow pressure pipelines using CFD numerical simulations and physical model experiments, analyzing changes in water phase volume fraction, water-gas two-phase flow patterns, and hydraulic parameters in the pipeline under low flow rate conditions of 0.6 m/s and high flow rate conditions of 1.5 m/s. Results show that under low flow rate conditions, there is more local trapped gas at the top of the pipeline, causing negative pressure at local high points in the pipeline and forming a vacuum. Under high velocity conditions, water-gas two-phase flow changes more frequently in the pipeline, with a large number of bubbles collapsing at the top, resulting in large fluctuations in pipeline pressure. Finally, through physical experiments, the main flow patterns during water filling in right-angle elbows are verified and analyzed. These results have certain reference significance for formulating safe and efficient water filling velocity schemes for pressurized pipelines.

Keywords: right-angle elbow; water filling process; water–air two-phase flow; numerical simulation; physical model experiment

1. Introduction

Water filling of pressurized water pipelines is an important part of long-distance water transmission projects. It occurs when water pipelines are first put into operation, when empty pipes are filled with water, when water supply is restored after maintenance, and when water supply is restored after troubleshooting. The pipelines reach stable operation through water filling [1–3]. The water filling process is a complex and dynamic hydraulic process that involves the interaction of water, air, and pressure. The pressure in the pipeline fluctuates greatly, resulting in a complex and changeable water-gas two-phase flow pattern. This directly affects the safe operation of the water supply system [4]. Many water supply projects to be built have the characteristics of long pipelines, large flows, and great elevation fluctuations [5]. In order to ensure the safe and efficient operation of water supply projects, many scholars have conducted numerical simulations and experimental research on the water filling process of pressurized water pipelines.

In a numerical simulation of the water filling process, both one-dimensional Method of Characteristics (MOC) models and three-dimensional Computational Fluid Dynamics

(CFD) models are commonly used to calculate unsteady flow. Within the one-dimensional calculation model, the rigid water column model and weak water column model are frequently employed [6], and many researchers have improved and optimized these models. Liu et al. [7,8] proposed a complete rigid model that incorporates local head loss, valve opening, and pipeline elevation changes, taking into account pipeline characteristics and establishing a mathematical model with variable characteristics suitable for long pipelines. Zhou et al. [9] introduced two variables, air release rate and water column length change, to perform numerical simulations and experimental verification of rapid water filling in horizontal pipelines. The theoretical value of pressure oscillation agrees well with experimental data when there is no hole or a small hole. Jin et al. [10] treated the water column as elastic in the elastic water column model, incorporating the propagation process of pressure waves in the water flow, resulting in more accurate numerical simulations of velocity and pressure in the pipeline. Zhou et al. [11] added water elasticity and gas compressibility characteristics to derive and establish a mathematical model of the pipeline water filling process containing stagnant air mass, which can accurately simulate the transient pressure of air mass in the pipeline. Wang [12] used the interface tracing method to verify that the elastic water column model is more applicable than the rigid water column model, with more practical simulation results for the pipeline water filling process. Compared to one-dimensional models, three-dimensional models can intuitively display the flow state of gas and water phases. Currently, the Volume of Fluid (VOF) model is the most commonly used multiphase flow model in pipeline water filling processes [13]. Feng et al. [14] used a VOF model to simulate water-gas two-phase flow in a pressurized pipeline of a pumping station, with simulation results showing an obvious transition phenomenon between flow patterns during the water filling process. Zhou et al. [15] used a VOF method to simulate the water filling process of a pipeline containing an air mass without deflation, with results showing that bottom flow first caused a sudden change in pressure, confirming the limitations of one-dimensional models and the advanced nature of VOF models. Bai et al. [16] used a VOF model to perform three-dimensional numerical simulations of concave pipelines, with result analysis showing that gas-liquid velocity differences in pipeline sections caused water-gas mixing. Warda et al. [17] used three-dimensional numerical calculations based on a VOF model to visually study phenomena such as column separation and reconnection in pipelines.

In terms of physical model experiments of the water filling process, Ciro et al. conducted a water filling experiment using a pipeline with a 30° inclination and proposed a standard for predicting maximum pressure fluctuations during rapid water filling [18]. Balacco et al. studied the dynamic characteristics of air valves during water filling under different boundary conditions for various pipeline layouts with pipeline inclination angles of 11°, 22°, and 30°, respectively [19]. Vasconcelos and Wright found that intercepted air directly impacts the shape of the leading edge of the water filling column after conducting water filling tests on pipes with different diameters, and that hydraulic jumps may occur during water filling [20]. Hou et al. performed an experimental study on two-phase pressurization moving characteristics during the rapid water filling process of large pipelines and found that the front edge of the flowing water phase did not completely fill the pipeline cross-section, with water flow being stratified and mixed [21]. Patrick et al. [22] conducted an experimental study on the influence of entrained air on pressure wave velocity in pipelines during rapid water filling using transparent closed PVC pipes with three different diameters and three different flow rates. Chen et al. [23] established a pipeline water filling simulation test system with an adjustable pipeline inclination range (0~30°) to address the air plug problem in undulating pipelines, with results showing that pipelines exhibit different flow patterns and hydraulic characteristics under different pipeline inclination angles. Guo et al. [24] performed a water-filling model test on a pipe section of approximately 5 km, with results showing that under existing vent design conditions, the influence of trapped bubbles on water delivery capacity could be ignored.

In summary, although some progress has been made in research on the water filling process of pressurized water pipelines, related research is not sufficient. In terms of numerical simulation, research on one-dimensional models is relatively mature, while research on three-dimensional numerical simulations mainly targets specific working conditions, with less research on unsteady flow characteristics of pipeline water filling processes [25]. In physical model tests, most tests are conducted under conditions of small diameter and low inclination, but there is no in-depth study on water filling tests of large diameter and high inclination. In terms of water filling velocity, it is generally believed that the water filling velocity should be between 0.3~0.6 m/s in engineering [26]. Currently, only the water filling velocity is about 0.3 m/s [27], but this water filling velocity is too small, greatly slowing down project completion progress. In this study, we provide insights into the water filling process of right-angle elbow pressurized pipelines using numerical simulations and physical model experiments. The characteristics of water–air two-phase transient flow are analyzed under two working conditions, with inlet water velocities of 0.6 m/s and 1.5 m/s, respectively.

2. Numerical Simulation of the Water Filling Process of Pressurized Pipeline

2.1. Model Development

As shown in Figure 1, we develop a geometric model of a pipeline which consists of a horizontal section at the left side of the pipeline, L1 = 2.2 m, a vertical upward section, L2 = 0.2 m, an upper horizontal section, L3 = 1.5 m, a vertical downward section, L4 = 0.2 m, and a horizontal section at the right side of the pipeline, L5 = 2.2 m, in which the left end of the pipeline is the water inlet, the upper horizontal section is an air inlet, the right end of the pipe is the outlet, and the rest are solid walls. The diameter of the pipeline is d = 0.2 m. As shown in Figure 2, our monitoring points P1, P2, P3, and P4 are selected to analyze the time evolution of the pressure in the pipeline.
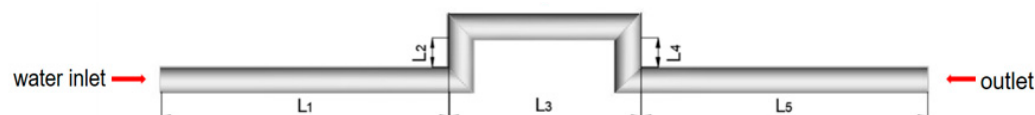

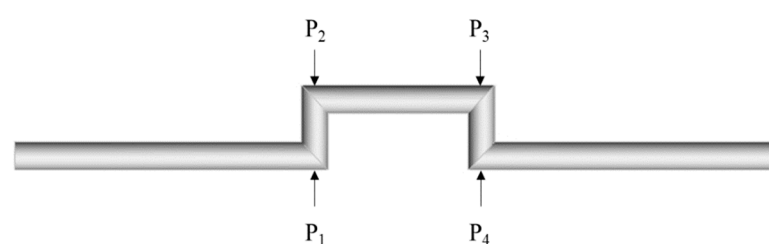**Figure 1.** Schematic diagram of the numerical model.

Figure 2. Layout of the monitoring points P1, P2, P3, and P4.

In this study, ICEM software is used to divide the grids. Since the model in the present study is a simple and regular three-dimensional cylindrical pipeline, the grid division is conducted using the O-shaped subdivision in ICEM and the grid's right-angle turning area is densified. The meshes of the numerical model is shown in Figure 3. In order to ensure the high accuracy of numerical simulation, the grid independence is verified by the pressure of P1 monitoring point under the steady condition of water inlet velocity of 0.6 m/s. The verification results of grid independence are shown in Figure 4. When the number of grids reaches 130,000, the data accuracy tends to be stable and the final number of grids is 137,802. The minimum value of grid orthogonal quality is 0.55.
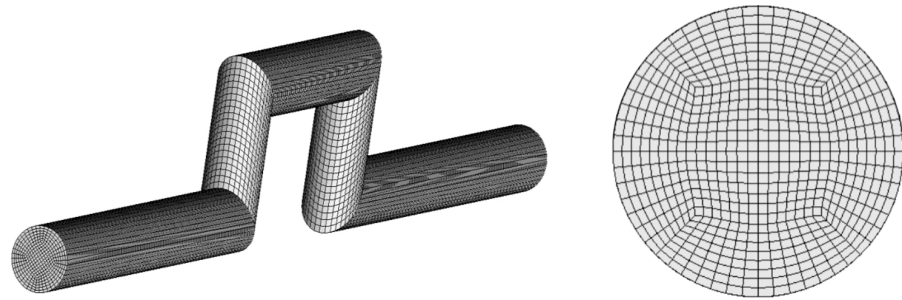
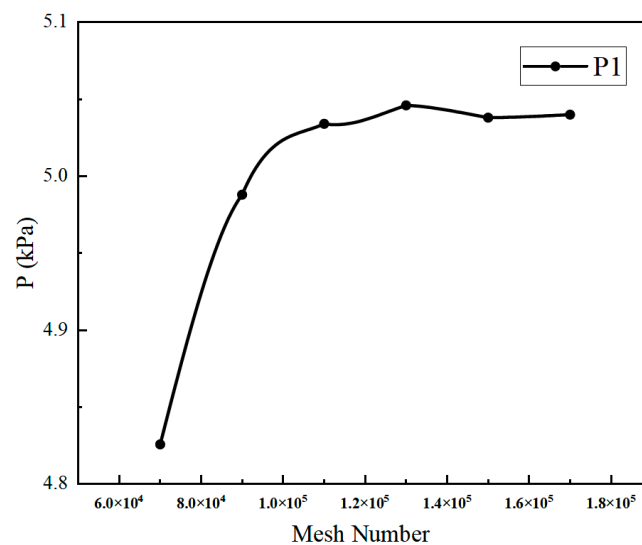**Figure 3.** The meshes of the numerical model.

Figure 4. Grid independence verification.

For the water filling process, the inlet of the pipeline is the velocity inlet, the inlet velocity is constant and independent with time, and the velocity value is set according to the needs of different working conditions. The outlet of the pipeline is connected to the atmosphere, the outlet boundary condition is set as the pressure outlet, and the pressure is the atmospheric pressure $p = 1.01 \times 10^5$ pa. In the process of pipeline filling water, the inlet of air is not considered; we thus assume that the boundary of the air inlet is same as the side wall. The standard wall function method is adopted to calculate the side wall of the pipe and no slip boundary conditions are adopted. The pipe system is insulated and has no heat exchange with the fluid. At the beginning of water filling process, the water volume fraction in the calculation area is set to 0, the relative humidity of air is 50%. The volume fraction at the boundary of the inlet is set to 1, indicating that the fluid at the inlet is the physical parameters of the water and air phases under the temperature of 20 °C. The standard atmospheric pressure is shown in Table 1.

Table 1. Physical parameters of water and air.

Fluid	Density (kg/m^3)	Dynamic Viscosity (pa·s)	Surface Tension (N/m)
Water	998.2	1.003×10^{-3}	0.072
Air	1.2	1.79×10^{-5}	0.072

2.2. Mathmatical Details of the Numerical Simulation

For the water–air two-phase transient flow in a pressurized pipeline, the proportions of air in the pipeline affect the flow characteristics. At present, the water–air two-phase flow in pipelines mainly include horizontal pipe flow and vertical pipe flow.

The flow patterns in horizontal pipes are generally asymmetric due to the influence of gravity of fluids with different densities. This leads to a vertical stratification, which means that the water tends to occupy the lower part of the pipe and force the air to flow upward. Specifically, it can be divided into seven types: bubble flow, plug flow, stratified smooth flow, stratified undulate flow, slug flow, annular flow, and spray flow. Compared with the two-phase flow pattern in a horizontal pipeline, the flow pattern of the two-phase flow in a vertical pipe is more symmetrical. It can be divided into six types: bubble flow, plug flow, slug flow, agitation flow, annular flow, and spray flow.

We use the standard k–ε turbulence model to establish a mathematical model for solving the water filling problem of the water–air two-phase flow in a pressurized pipeline. The control equations are as follows:

1.　Continuity equation

$$\frac{\partial \rho}{\partial t} + \nabla(\rho u) = 0 \tag{1}$$

Since the water–air two-phase fluid exist simultaneously in each grid, the continuity equation can be expanded as:

$$\frac{\partial}{\partial t}\left(\alpha_g \rho_g\right) + \nabla \cdot \left(\alpha_g \rho_g u_g\right) = 0 \tag{2}$$

$$\frac{\partial}{\partial t}\left(\alpha_l \rho_l\right) + \nabla \cdot \left(\alpha_l \rho_l u_l\right) = 0 \tag{3}$$

$$\alpha_g + \alpha_l = 1 \tag{4}$$

2.　Momentum equation

$$\frac{\partial(\rho u)}{\partial t} + \nabla(\rho u u) = -\nabla p + \nabla\left[\mu\left(\nabla u + \nabla u^T\right)\right] + \rho g + F \tag{5}$$

3.　Energy equation

$$\frac{\partial\left(\alpha_p T\right)}{\partial t} + \nabla \cdot \left(\alpha_p U T\right) = \nabla \cdot (\lambda \nabla T) + S_T \tag{6}$$

where α_l, α_g are the volume fractions of the liquid (water) and gas (air) phases; u_l, u_g are the velocities of the liquid phase (water) and gas phase (air), m/s; ρ_l, ρ_g are the densities of the liquid phase (water) and the gas phase (air), kg/m^3; t is time, s; μ is the dynamic viscosity coefficient; g is the gravitational acceleration, m/s^2; F is the volumetric force, N; p is the pressure, Pa; T is the temperature, °C; S_T is the source term.

By solving the continuity equation, the position of the interface of two phases and the proportions of water and gas in each grid can be obtained. The hydraulic parameters including the pressure and velocity of water and gas can be obtained by solving the momentum equation and energy equation.

4.　Turbulence equation

Turbulent kinetic energy *k* equation:

$$\frac{\partial(\rho k)}{\partial t} + \frac{\partial(\rho k u_i)}{\partial x_i} = \frac{\partial}{\partial x_j}\left(\left(\mu + \frac{\mu_t}{\sigma_k}\right)\frac{\partial k}{\partial x_j}\right) + G_k + G_b - \alpha\varepsilon - Y_m + S_k \tag{7}$$

where σ_k is the turbulent Ludwig Prandtl number corresponding to turbulent kinetic energy k, which is taken by default as $\sigma_k = 1.0$; μ is the dynamic viscosity coefficient; G_k represents the generation term of turbulent kinetic energy k caused by the average velocity gradient; G_b represents the generation term of turbulent kinetic energy k caused by buoyancy; Y_m represents the effect of compressible turbulent pulsation expansion on the total dissipation rate; g is the gravitational acceleration, m/s^2; S_k is the source term.

The finite volume method, which has been commonly used to solve the governing equations of two-phase flow, is selected to simulate the water filling process of the pressurized pipeline. The transient hydraulic calculation is carried out based on the pressure transient solver. In order to ensure the accuracy of the calculation, the three-dimensional and double precision calculation mode is selected. The most widely used standard k-1 ε turbulence model is selected as the turbulence model. For the pressure velocity coupling method, we adopt the pressure implicit with splitting of operators (PISO) algorithm, which is proficient at solving transient problems. The gradient term is given based on the element volume least square method. The volume force weighting format is selected as the pressure interpolation format. The geo reconstruct format is selected for volume fraction interpolation, which can accurately track the calculation format of the interface of the water–air two-phase flow. The second-order upwind scheme is selected for the interpolation schemes of the continuity equation, momentum equation, turbulence equation, and energy equation. By verifying the grid-independent solution, we finally select 130,000 grids.

2.3. Results of the Numerical Simulation

Based on the three-dimensional numerical model that has been proposed in the above section, we select two working conditions with the inlet water flow velocity set to 0.6 m/s (named as case 1) and 1.5 m/s (named as case 2), respectively. The characteristics of the water–air two-phase transient flow in the pipeline are observed under these two working conditions.

We first determine the water–air two-phase transient flow state in the pipeline at varying time. Figures 5 and 6 illustrate the time variation of the water–air interaction under the working condition of case 1 and case 2, respectively. The red parts represent the water flow, the blue parts denote the air bag, and the green parts represent large air bubbles.
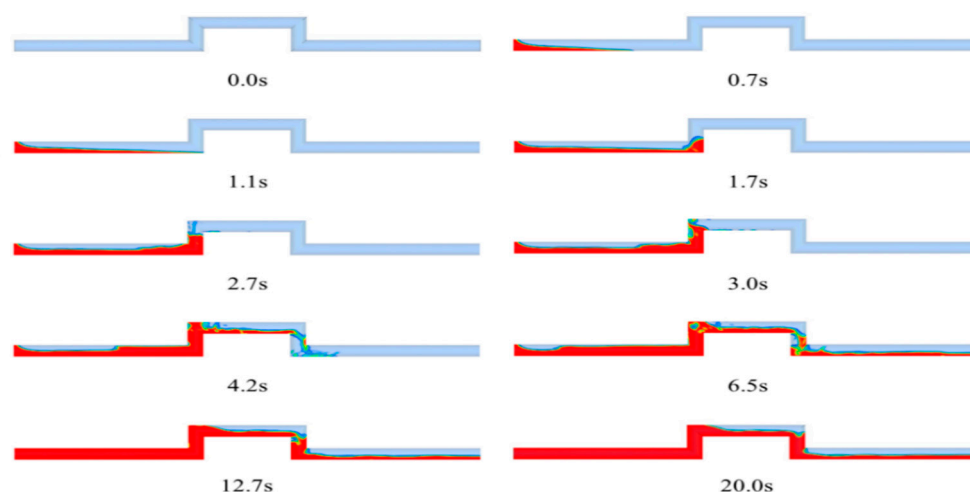

Figure 5. Time variation of the water–air interaction under the working condition of case 1 obtained from numerical simulation.
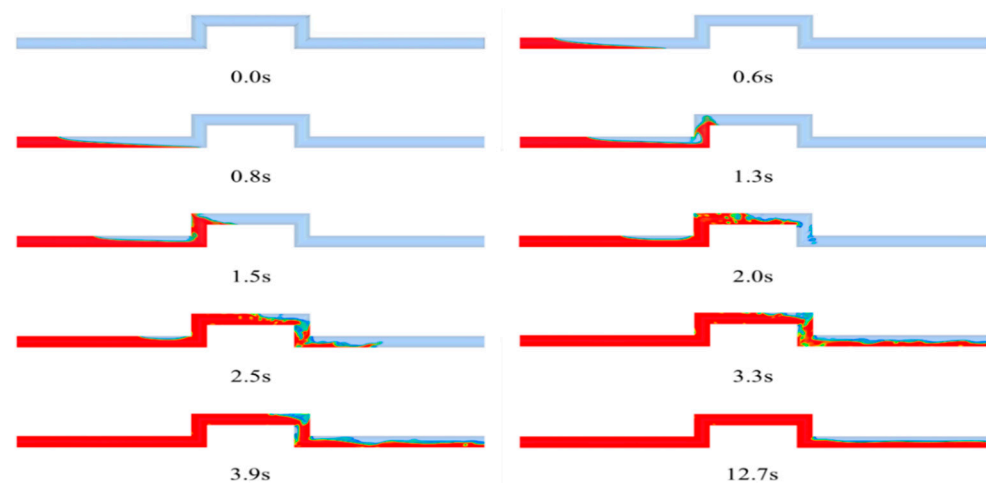
Figure 6. Time variation of the water–air interaction under the working condition of case 2 obtained from numerical simulation.

By comparing the water filling process under two different working conditions, it can be seen that the time required for water filling process decreases with the increase of water filling velocity. From the perspective of gas stagnation in the pipeline, with the increase of flow rate, the air retained in the pipeline decreases. When the speed reaches 1.5 m/s, except for the horizontal pipe section L5, all other sections of the pipelines are filled with water.

Water filling is a process in which the volume fraction of the water phase changes with time. Figure 7 shows the time evolution of the volume fraction of the water phase under case 1 and case 2. Equations (8) and (9) are fitting functions for the curve of water phase volume fraction with time.

$$y = \begin{cases} 0.089t & 0 \le t < 5.7 \\ 6 \times 10^{-5}t^3 + 0.0034t^2 + 0.0661t + 0.2398 & 5.7 \le t < 18.6 \\ 0.69 & t \ge 18.6 \end{cases} \tag{8}$$

$$y = \begin{cases} 0.149t & 0 \le t < 4.1 \\ 6 \times 10^{-5}t^3 + 0.0028t^2 + 0.0491t + 0.4656 & 4.1 \le t < 16.7 \\ 0.69 & t \ge 16.7 \end{cases} \tag{9}$$
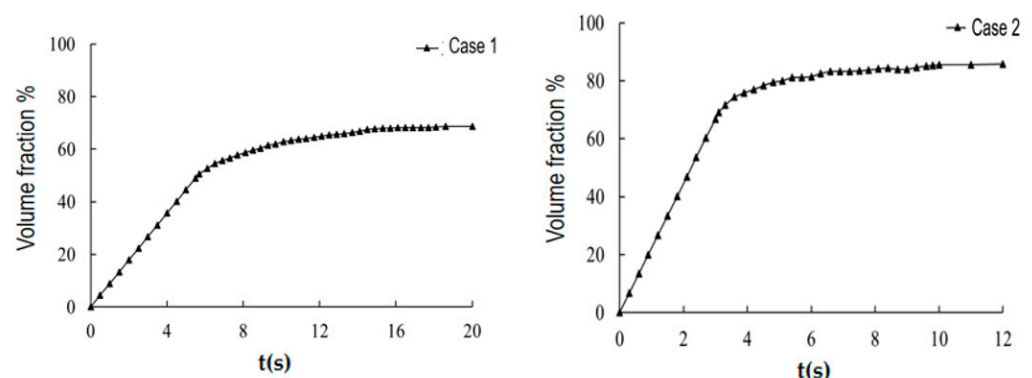

Figure 7. Time variation of the volume fraction of the water phase for case 1 and case 2.

In order to facilitate the observation of the flow pattern changes of water and gas at different times during the water filling process, the central sectional views of the pipeline with the same flow direction are shown in Figure 8, where the red parts denote the water phase and the blue parts represent the air phase. It can be seen from Figure 7 that the

flow patterns in the pipeline water filling process under case 1 include stratified flow, plug flow, bubble flow, slug flow, and wavy flow. Due to the slow water filling flow rate, the mutual conversion of different flow patterns is also slow. The flow patterns in the process of pipeline water filling under case 2 include stratified flow, plug flow, bubble flow, slug flow, and wavy flow. In this case, the conversion of different flow patterns is very frequent.
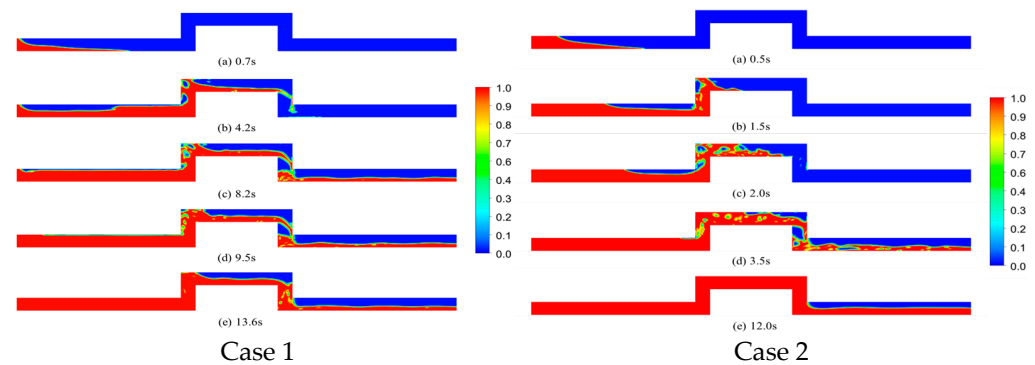

Figure 8. Water–air two-phase flow pattern of the pipeline.

According to the flow patterns of the water–air two-phase flow observed in the pipeline, we select the flow state of case 1 as an example and analyze the velocity field during the water filling process. Figure 9 is a velocity vector diagram of the two-dimensional plane flow field along the flow direction of the pipeline, and Figure 10 is a partial image of the flow field. The difference of the velocity vector arrow size in the velocity vector diagram shows the difference of its velocity. The larger the arrow, the greater the flow velocity. The dense arrows and the twisted streamline direction indicate that the area is chaotic. It is noted that the velocity field and streamline distribution of the stratified flow and wavy flow are uniform and close to linearity. As the sizes of bubbles in the bubble flow are relatively small, the motion of the air bubbles has a very small effect on the streamline and flow direction of the flow pattern. For plug flow, the oscillation of large air bubbles carried in the aqueous phase makes the streamline of the flow pattern wavy and distorted, and the velocity direction changes significantly. In the slug flow, as the air bag with a large volume fraction is retained in the flow pattern and the water phase overflow area is greatly reduced, the distribution of the streamline of the water phase is relatively dense. The gas phase in the air bag moves, driven by the water phase, and its streamline generates vortices. In addition, an obvious velocity gradient is observed at the intersection of water and air on the flow field vector diagram of the pipeline.
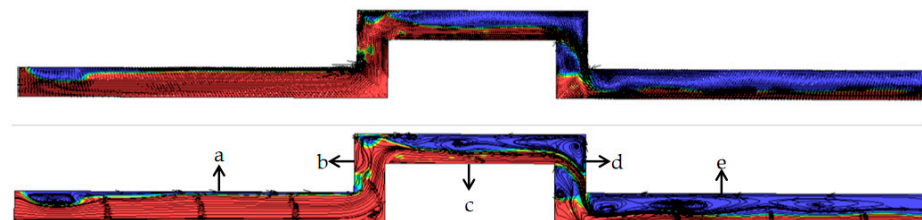

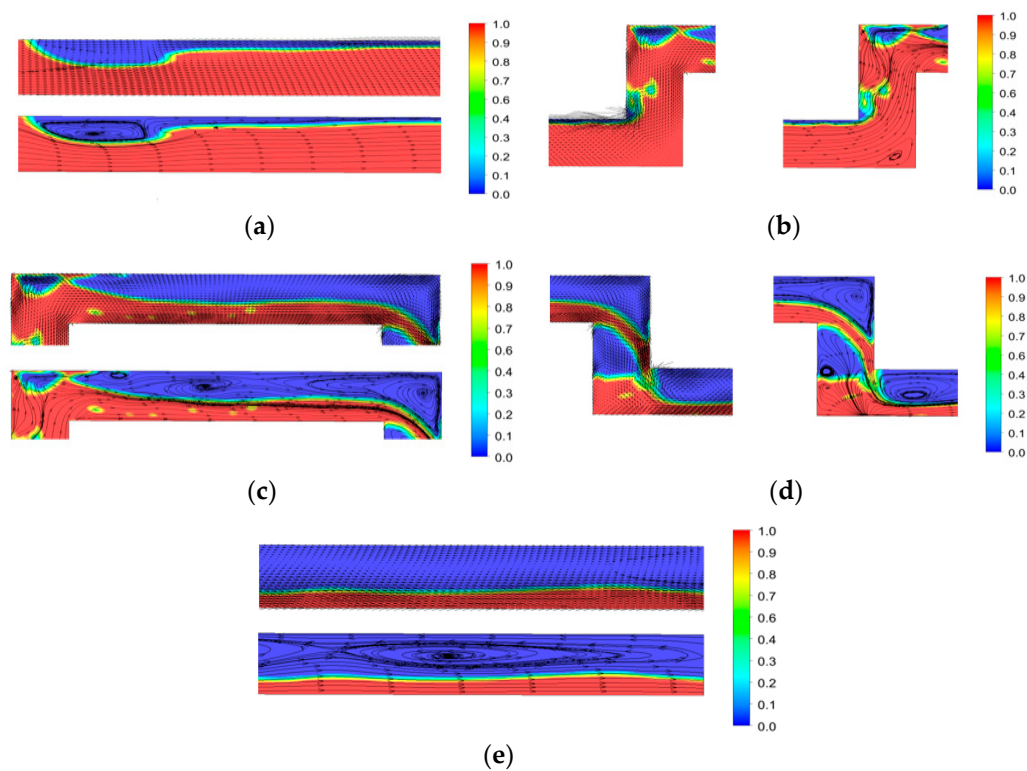**Figure 9.** Pipeline velocity vector diagram (**upper**) and streamline diagram (**lower**).

Figure 10. Local velocity vector diagram and streamline diagram. (**a**) a horizontal section at the left side, (**b**) a vertical upward section, (**c**) an upper horizontal section, (**d**) a vertical downward section, (**e**) a horizontal section at the right side.

Figure 11 illustrates the time evolution of the relative pressure at the indicated four monitoring points. At the beginning of water filling process, the air that remains in horizontal pipe (i.e., section L1 in Figure 1) affects the variation of pressure in the pipeline. The greater the amount of air, the more intense the pressure variation in the vertical upward pipe (i.e., section L2), and the greater the fluctuation range. In addition, the water filling velocity is an important factor affecting the pressure in the pipeline. By comparing the pressure under these two working conditions, it can be seen that a small water filling velocity causes negative pressure at the high points of the pipeline. The greater the water filling velocity, the higher the maximum pressure in the pipeline, and the greater the stable pressure when the water flow is relatively stable. However, the maximum and minimum pressure in the pipeline under the water filling flow rate conditions are within the pressure bearing range of the pipeline. Therefore, for the water transmission pipeline like the right-angle elbow model, in order to shorten the water filling cycle and reduce the retention of air at local high points after water filling, the water filling velocity can be increased under the condition of ensuring the safety of the pipeline.
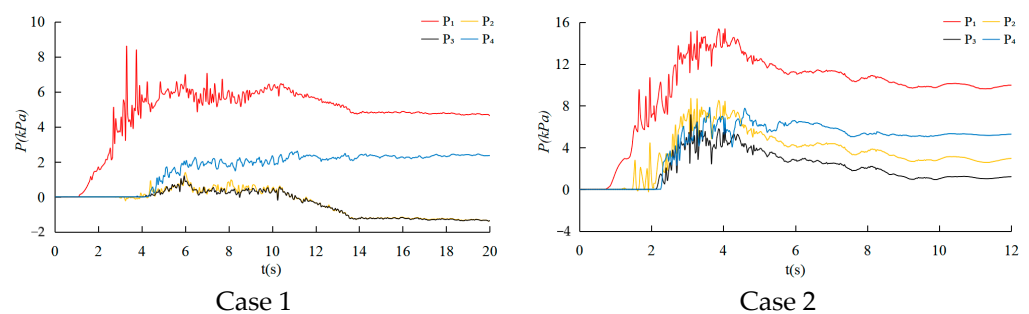

Figure 11. Time variation of the pressure at different monitoring points for case 1 and case 2.

3. Physical Model Experiments

3.1. Experimental Method

The water–air two-phase transient flow test system mainly includes a water supply module, air supply module, and data acquisition module. The experimental facilities are shown in Figure 12. The facilities are established to study complex two-phase flow in the pressurized pipeline in water supply systems. The water supply module is established to control the water filling velocity in the pipeline, where the water pump used in experiments is a horizontal pipeline centrifugal pump with variable frequency. For the air supply module, to provide different flow streams and ensure the control accuracy of the gas flow, three parallel pipelines are designed to connect gas flow meters with different ranges. One gas pipeline can be selected, the other two pipelines are closed, and the gas flow can be finely adjusted through the cooperation of the valve and flow meter. Pipelines with multi-inclination and multiple diameters are established. The water and air are mixed and transported into different types of two-phase flow by connecting the water supply and gas supply modules through multi-line pipelines.
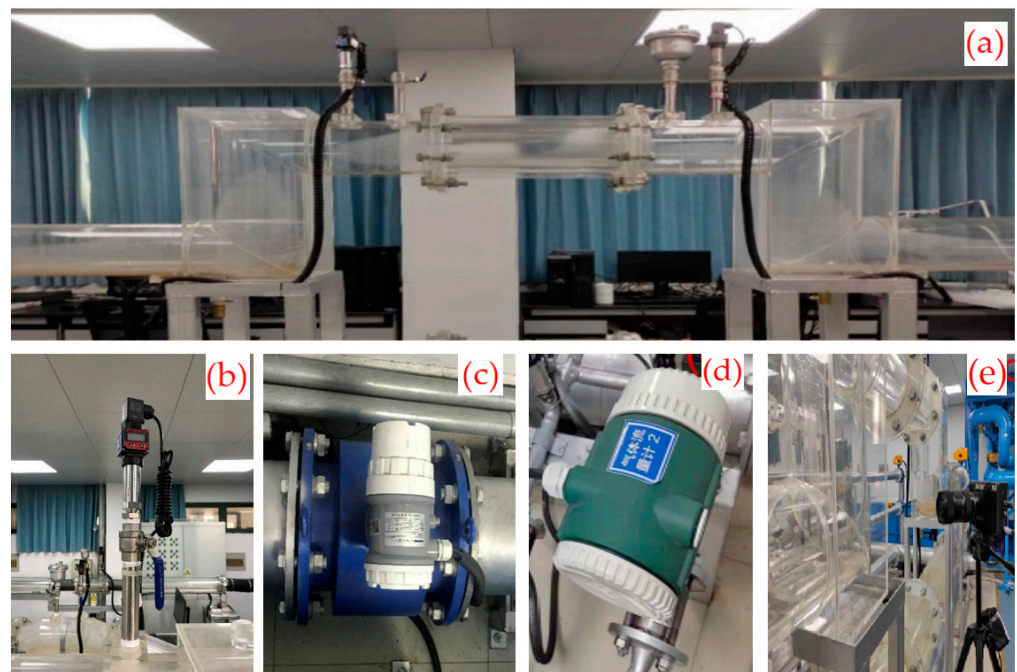

Figure 12. Experimental facilities: (**a**) pipeline, (**b**) the reassure measurement system, (**c**) the water flow measurement system, (**d**) the air flow measurement system, (**e**) high speed camera.

The data acquisition module consists of three parts: the reassure measurement system, flow measurement system, and image acquisition system. The reassure measurement system is shown in Figure 12b. Multiple sets of pressure measurement components are used to monitor the pressure in the pipeline in real time. Among them, the intelligent pressure transmitter with the model of hr3202 is used, with a range of 0~1.6 Mpa, accuracy of 0.5% FS, output of a 4~20 mA current signal, a power supply of 12–24 VCD, and a pressure sensor customized by Shaanxi Hengrui Measurement and Control System Company. For the water flow measurement system, the MGG / KL electromagnetic flowmeter is adopted. Its main parameters are accuracy ±0.3% R, velocity measurement range 0.1~15 m/s, velocity resolution 0.5 mm/s, which is customized by Jiangsu Chuanghui Braking Instrument Company. Its layout is shown in Figure 12c. For the air flow measurement system, the CH-LU20F vortex flowmeter is adopted. Its measuring range is 8~800 L/min, the accuracy is 1.5%, the output model is 4–20 mA, and the power supply is 24 V, which is customized by Jiangsu Chuanghui Braking Instrument Company. Its layout is shown in Figure 12d. For the image acquisition system, the high-speed high-definition camera FASTEC IL5 is used,

and the electronic shutter speed of high-speed high-definition camera is 3 microseconds to 41.667 milliseconds, which can track the operation state of the gas–liquid two-phase flow test through image acquisition at a high acquisition frequency. The image acquisition is shown in Figure 12e.

3.2. Experimental Results

The experiments mimic the water filling process of a pressurized pipeline with a right-angle elbow with a diameter of DN200 and a water filling flow rate of 0.6 m/s and 1.5 m/s. When the water filling velocity at the inlet of the pipeline is 0.6 m/s, the water–gas two-phase flow pattern image of each part in the two-phase flow observation section is as shown in Figure 13.
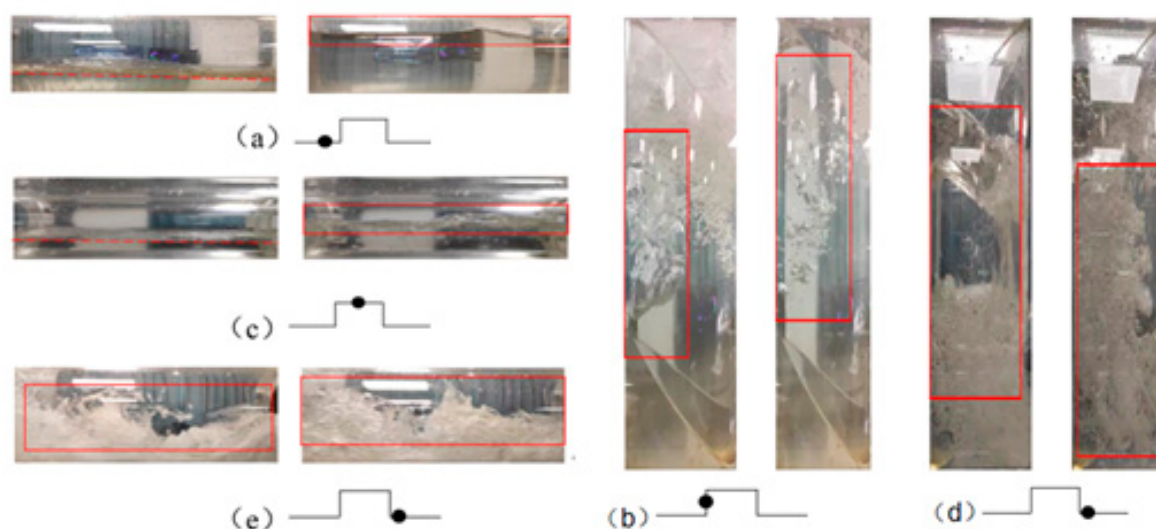

Figure 13. Two-phase flow pattern distribution of each pipe section (flow rate 0.6 m/s).

When the water filling velocity at the inlet of the pipeline is 1.5 m/s, the water–gas two-phase flow pattern image of each part in the two-phase flow observation section is as shown in Figure 14.
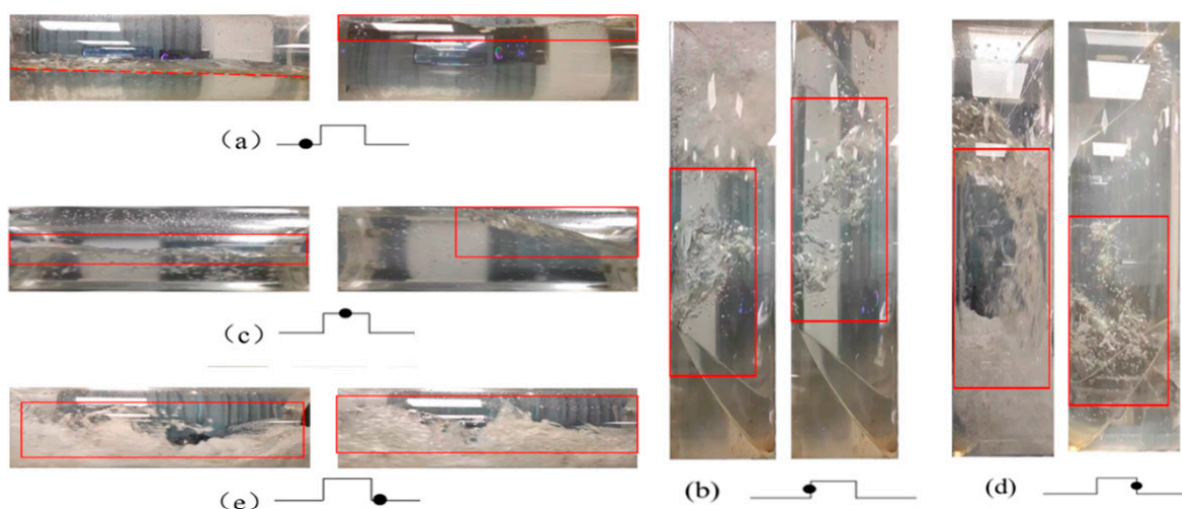

Figure 14. Two-phase flow pattern distribution of each pipe section (flow rate 1.5 m/s).

Figure 15 indicates the time variation of the pressure at the four indicated monitoring points with the water filling velocity at the inlet of the pipeline is 0.6 m/s and 1.5 m/s,

respectively. It can be seen that the largest pressure fluctuation in the two working conditions appears at the monitoring point P1. When the flow rate is 0.6 m/s, the pressure fluctuation at P1 is significantly greater than that under the flow rate of 1.5 m/s. The overall pressure at P1 is significantly greater than the former. With a flow rate of 0.6 m/s, the time evolution curves of the pressure at monitoring points P2 and P3 fluctuate and rise at the very beginning, and then slowly decline. The varying tendencies of pressure are basically the same with different flow rates, and finally the pressure is basically stable in the state of negative pressure. Under the water filling condition with the flow rate of 1.5 m/s, the pressure curves at monitoring points P2 and P3 vary obviously, and there is no negative pressure.
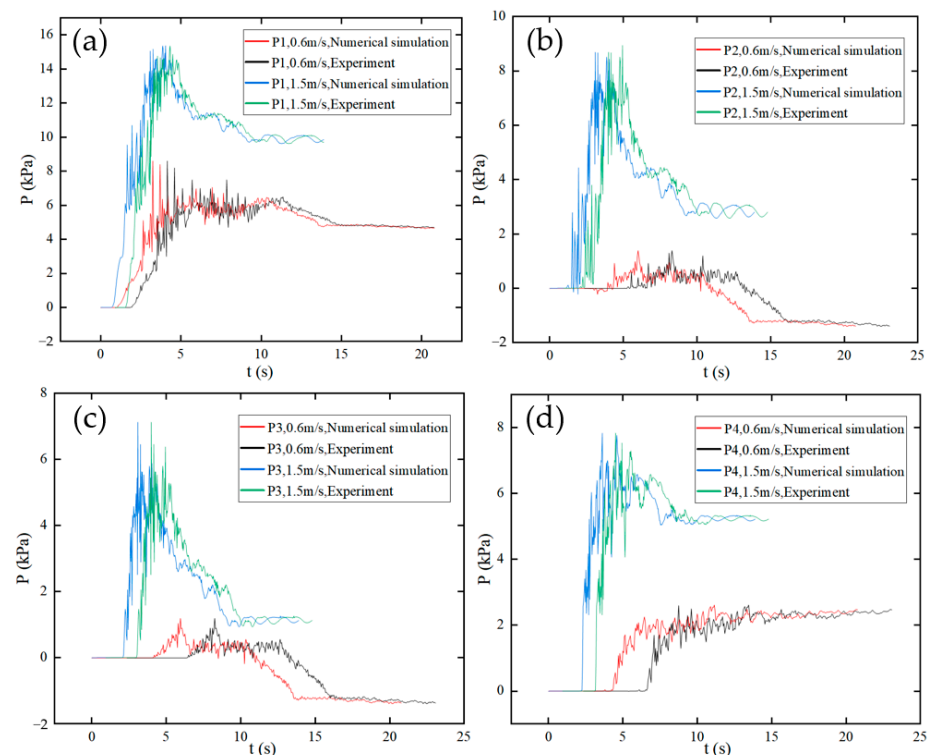

Figure 15. Time evolution of the pressure at the four indicated monitoring points: (**a**) P1 monitoring point, (**b**) P2 monitoring point, (**c**) P3 monitoring point, (**d**) P4 monitoring point.

3.3. Comparison of Experimental Results and Numerical Simulation Results

As shown in Table 2, for the two working conditions with flow rates of 0.6 m/s and 1.5 m/s, the water–air two-phase flow patterns obtained from physical model experiments are compared with numerical simulation results. By comparing the two-phase flow patterns, we observed stratified flow, wavy flow, plug flow, bubble flow, and slug flow both in numerical simulation and experiments, the appearance time and structure distribution of each flow pattern are very consistent. For the pressure change of each monitoring point during water filling, it can be seen that the experimental results obviously lag behind the numerical simulation, which is caused by ignoring the friction resistance of the pipeline in the numerical simulation process. The overall pressure change law is very similar, and the pressure value of the experimental results is slightly higher than that of the numerical simulation. Additionally, with the increase in the water filling velocity, the interaction between the water and gas is more intense and the flow pattern changes more frequently.

Table 2. Comparison of numerical and experimental results under different working conditions.

Condition	Inlet Velocity (m/s)	Calculated Pressure (kPa)	Measured Pressure (kPa)	Error (%)
Water filling	Velocity 0.6 m/s	8.60	8.48	1.39
Water filling	Velocity 1.5 m/s	15.37	14.86	3.32

4. Conclusions

This study provides insights into the water filling process of right-angle elbow pressurized pipelines using numerical simulations and physical model experiments. The characteristics of water–air two-phase transient flow are analyzed under two working conditions with inlet water velocities of 0.6 m/s and 1.5 m/s, respectively. The main conclusions and prospects are as follows:

(1) Under low flow rate conditions, there is more local trapped gas at the top of the pipeline, causing negative pressure at local high points in the pipeline. Under high velocity conditions, there is no gas stagnation at local high points in the pipeline, with a large number of bubbles collapsing at the top of the pipeline, causing large fluctuations in pipeline pressure. Therefore, in practical engineering, air valves should be installed at local high points in water pipelines to not only discharge trapped gas but also allow gas to enter when there is negative pressure in the pipeline.

(2) The main flow patterns during the water filling process of right-angle elbow pipelines include stratified flow, slug flow, bubble flow, plug flow, and wavy flow. The larger the water filling velocity, the more frequent the conversion of water–air two-phase flow patterns in the pipeline. Pipeline pressure changes violently due to slug flow.

(3) The pipeline water filling process can be divided into two stages. In the first stage, flow patterns and pressure in the pipeline change dramatically, while in the second stage, flow patterns and pressure in the pipeline gradually stabilize. Based on this principle, a phased water filling method can be adopted in practical engineering to effectively reduce pressure peaks and shorten water filling time.

Author Contributions: Conceptualization, J.H. and Y.Z.; methodology, J.H., Q.W. and J.Z.; software, J.H., Q.W. and Z.M.; validation, Z.M.; formal analysis, J.H.; investigation, J.H.; resources, J.H.; data curation, J.Z.; writing—original draft, J.H. and Y.Z.; writing—review and editing, J.H., Q.W. and Z.M. visualization, J.F.; supervision, Q.W.; project administration, J.H.; funding acquisition, J.H. All authors have read and agreed to the published version of the manuscript.

Data Availability Statement: The numerical simulation data and experimental data used to support the findings of this study are available from the corresponding author upon request.

Conflicts of Interest: The authors declare no conflict of interest.

References

1. Guo, Y.X.; Wu, H.T.; Yang, K.; Guo, X.L.; Wang, T. Analysis of Dynamic Characteristics of Gas-liquid Flow During Water-filling Process in Pipeline. *S-N Water Transf. Water Sci. Tech.* **2013**, *11*, 65–69.
2. Li, L.; Zhu, D.Z.; Huang, B. Analysis of Pressure Transient Following Rapid Filling of a Vented Horizontal Pipe. *Water* **2018**, *10*, 1698. [CrossRef]
3. Zhang, J.; Zhu, X.Q.; Qu, X.H.; Ma, S.B. Arrangement of air-valve for water hammer protection in long-distance pipelines. *J. Hydraul. Eng.* **2011**, *39*, 1025–1033. [CrossRef]
4. Liu, J.; Xu, D.; Zhang, S.; Bai, M. Experimental and Numerical Study on Water Filling and Air Expelling Process in a Pipe with Multiple Air Valves under Water Slow Filling Condition. *Water* **2019**, *11*, 2511. [CrossRef]

5.　Shi, L.; Zhang, J.; Ni, W.X.; Chen, X.Y.; Li, M. Water Hammer Protection of Long-Distance Water Supply Project with Special Terrain Conditions. *J. Hydraulic. Eng.* **2019**, *38*, 81–88. [CrossRef]

6.　Wang, F.J.; Wang, L. Research progress of transient flow in water filling process of large pipeline water conveyance system. *J. Hydraulic. Eng.* **2017**, *36*, 12. [CrossRef]

7.　Liu, D.Y.; Suo, L.S. Rigid mathematical model of air mass trapped in pipeline impacted by water flow. *Adv. Water Sci.* **2004**, *15*, 6. [CrossRef]

8.　Liu, D.Y.; Suo, L.S. Rigid mathematical model of water flow impacting air mass in long pipeline with variable characteristics. *Res. Pro. Hydrodyn.* **2005**, *20*, 6. [CrossRef]

9.　Zhou, L.; Liu, D.Y.; Karney, B.; Zhang, Q.F. Influence of Entrapped Air Pockets on Hydraulic Transients in Water Pipelines. *J. Hydraul. Eng.* **2011**, *137*, 1686–1692. [CrossRef]

10.　Jin, Z.; Jiang, N.C.; Wang, X.H. *Pump Stop Water Hammer and Its Protection*, 2nd ed.; China Building Industry Press: Beijing, China, 2004; ISBN 978-71-1206-274-4.

11.　Zhou, L.; Liu, J.; Huang, K.; Liu, D.Y. Numerical simulation of transient flow with trapped air mass during start-up and filling of water pipeline. *Adv. Sci. Tech. Water Resour.* **2021**, *41*, 1–7.

12.　Wang, L. Numerical Study on Transient Flow of Rapid Water Filling in Pipeline. Ph.D. Thesis, China Agricultural University, Beijing, China, 2017.

13.　Liu, B. *Fluent 19.0 Fluid Simulation from Entry to Mastery*; Tsinghua University Press: Beijing, China, 2019; ISBN 978-73-0252-575-2.

14.　Feng, L.; Yao, Q.Y. Numerical simulation of gas-liquid two-phase flow in pressure pipeline of pumping station based on VOF model. *China Rural Water Hydropower* **2012**, *12*, 124–126.

15.　Zhou, L.; Liu, D.Y.; Chuan, Q. Simulation of Flow Transients in a Water Filling Pipe Containing Entrapped Air Pocket with VOF Model. *Eng. Appl. Compu. Flu. Mech.* **2014**, *5*, 127–140. [CrossRef]

16.　Bai, R.Y.; Bao, J.W.; Song, L. Transient numerical simulation analysis of gas-liquid two-phase flow in municipal water supply pipeline under water filling and exhaust conditions. *J. Inner. Mong. Uni. Tech.* **2017**, *36*, 9. [CrossRef]

17.　Warda, H.A.; Wahba, E.M.; Salah El-Din, M. Computational Fluid Dynamics (CFD) simulation of liquid column separation in pipe transients. *Ale. Eng. J.* **2020**, *59*, 3451–3462. [CrossRef]

18.　Apollonio, G.; Balacco, G.; Fontana, N.; Giugni, M.; Marini, G.; Piccinni, A.F. Hydraulic Transients Caused by Air Expulsion During Rapid Filling of Undulating Pipelines. *Water* **2016**, *8*, 25. [CrossRef]

19.　Balacco, G.; Apollonio, C.; Piccinni, A.F. Experimental analysis of air valve behaviour during hydraulic transients. *J. Appl. Water Engi. Res.* **2015**, *3*, 1–3. [CrossRef]

20.　Vasconcelos, J.; Wright, S. Investigation of rapid filling of poorly ventilated stormwater storage tunnels. *J. Hydra. Res.* **2009**, *47*, 547–558. [CrossRef]

21.　Hou, Q.; Tijsseling, A.S.; Laanearu, J.; Annus, I.; Koppel, T.; Bergant, A.; Vučković, J.; Anderson, A.; Jos, M.C. Experimental investigation on rapid filling of a large–scale pipeline. *J. Eind. Uni. Tech.* **2013**, *1335*, 1–27. [CrossRef]

22.　Patrick, A.C.; Vasconcelos, J.G. Air Entrainment Effects on the Pressure Wave Celerities Following Rapid Filling Pipe Flows. In Proceedings of the World Environmental and Water Resources Congress, Austin, TX, USA, 17—21 May 2015; pp. 1638–1647. [CrossRef]

23.　Chen, Y.Y.; Chui, Y.Y.; Yu, D.; Gong, J. Loop system for simulation test of water filling and exhaust of pipeline containing gas plug. *Res. Explor. Labor* **2019**, *38*, 42–46. [CrossRef]

24.　Guo, Y.X.; Yang, K.L.; Guo, X.L.; Fu, H. Influence of retained bubbles on water delivery capacity during water filling of large pipeline water delivery system. *J. Hydra. Eng.* **2013**, *44*, 262–267. [CrossRef]

25.　Du, Y.Z.; Chen, Y.C.; Li, W.Q.; Liu, D.C.; Song, T.N. Introduction of Water Passing Test of Mopanshan Water Transfer Project in Harbin. *Water Supply Drain.* **2009**, *14*, 12–14. [CrossRef]

26.　American Water Works Association. *Concrete Pressure Pipe: M9—1995*; American Water Works Association: New York, NY, USA, 1995.

27.　Wang, L.; Wang, F.J.; Huang, J. Numerical investigation of filling transients in small-scale pipelines with submerged outlet. *J. Hydrodyn.* **2019**, *31*, 1–7. [CrossRef]